Lithium Polymer Battery State-of-Charge Estimation Based on Adaptive Unscented Kalman Filter and Support Vector Machine

Jinhao Meng, *Student Member, IEEE*, Guangzhao Luo, *Member, IEEE*, and Fei Gao, *Senior Member, IEEE*

***Abstract*—An accurate algorithm for lithium polymer battery state-of-charge (SOC) estimation is proposed based on adaptive unscented Kalman filters (AUKF) and least-square support vector machines (LSSVM). A novel approach using the moving window method is applied, with AUKF and LSSVM to accurately establish the battery model with limited initial training samples. The effectiveness of the moving window modeling method is validated by both simulations and lithium polymer battery experimental results. The measurement equation of the proposed AUKF method is established by the LSSVM battery model and AUKF has the advantage of adaptively adjusting noise covariance during the estimation process. In addition, the developed LSSVM model is continuously updated online with new samples during the battery operation, in order to minimize the influence of the changes in battery internal characteristics on modeling accuracy and estimation results after a period of operation. Finally, a comparison of accuracy and performance between the AUKF and UKF is made. Simulation and experiment results indicate that the proposed algorithm is capable of predicting lithium battery SOC with a limited number of initial training samples.**

***Index Terms*—Adaptive unscented Kalman filter (AUKF), least-square support vector machine (LSSVM), Lithium polymer battery, modeling, moving window method, state of charge (SOC).**

I. Introduction

LITHIUM batteries have been widely used as the power supply source in various applications, such as portable devices, electrified transportation [1], etc. Due to their superior energy density, preferable power-to-energy balance, and long cycle life, lithium polymer batteries are applied to electric vehicles (EVs) and hybrid electric vehicles (HEVs) [2]. The battery management system (BMS) is needed to guarantee battery safety, extend its operational life and enable it to meet the demands of EVs. In general, battery state estimation is one of the key issues in BMS [3]. The battery state-of-charge (SOC) indicates the amount of electrical energy left. Depending on the battery SOC, BMS selects the control strategy of a discharging or charging current in an electrical circuit [4]. Thus, an appropriate SOC can assist BMS to avoid overcharging and unbalancing circumstances among batteries in the pack [5]. However, SOC can only be estimated from battery terminal characteristics due to the fact that a lithium battery itself is an enclosed system. With SOC as a crucial parameter in the BMS, battery SOC estimation has received considerable attention in recent years.

The conventional methods for SOC estimation include Ampere hour counting or coulomb counting [6], open-circuit voltage estimation [7], artificial neural networks [8], and others [9]–[12], all of which can be adopted to complete the SOC estimation process and obtain acceptable results in different applications. Ampere hour counting and open-circuit voltage estimation are the most common methods for SOC estimation. However, the essential of initial SOC makes it difficult for Ampere hour counting to be applied to practice. Furthermore, due to the accumulation of measurement errors, the method inevitably results in inaccuracy. For open-circuit voltage estimation, a long time (up to hours) is needed for a battery to be relaxed to reach its equilibrium, which makes this method hardly available for online applications. Therefore, it is suitable as an SOC estimation method merely at the beginning or end of the entire process.

In order to compensate estimation errors and obtain accurate SOC, there has been an increasing interest in observe-based methods [13]. Although the main drawback is their computational burden, Kalman filter-based methods prove to be an efficient algorithm to improve SOC estimation accuracy [14]–[17] [19]–[21]. The Kalman filter is widely used in system state estimation and has achieved expected efficiency and performance in many applications, such as aerospace, military, and other areas. When SOC is estimated by Kalman filter-based methods, it is necessary to build the state-space equation of the battery at first. In the condition of minimum mean square error, Kalman filter makes full use of the previous and the current results to achieve optimal estimation of current state variables. However, the estimation process of battery SOC inevitably results in errors because the Kalman filter is only suitable for linear systems while battery charging and discharging are complex nonlinear processes. The extended Kalman filter (EKF), which linearizes the state-space equation of nonlinear systems by Taylor's formula, has received better results on SOC estimation [14]–[17]. However, the iterative process of the EKF will yield linearization errors as a result of ignoring higher order terms of Taylor's formula. The nonlinear matrix of the state-space equation may be nondifferentiable, that is, the Jacobian matrix may not be calculated in some cases. As a matter of fact, the Jacobian matrix, the

Manuscript received December 4, 2014; revised February 16, 2015 and April 14, 2015; accepted May 20, 2015. Date of publication June 1, 2015; date of current version November 16, 2015. This work was supported by the General Project of the National Natural Science Foundation of China (51177135). Recommended for publication by Associate Editor S. Williamson. *(Corresponding author: Guangzhao Luo.)*

J. Meng and G. Luo are with School of Automation, Northwestern Polytechnical University (NPU), Xi' an 710072, China (e-mail: scmjh2008@163.com; guangzhao.luo@nwpu.edu.cn).

F. Gao is with the University of Technology of Belfort-Montbéliard, Belfort 90000, France (e-mail: fei.gao@utbm.fr).

Color versions of one or more of the figures in this paper are available online at http://ieeexplore.ieee.org.

Digital Object Identifier 10.1109/TPEL.2015.2439578

computation results of first-order partial derivative of the system matrix, is required in the calculation of EKF. Therefore, in order to make up the shortcomings of EKF, the unscented Kalman filter (UKF) based on the unscented transform is proposed. The research in [18] indicates that the UKF is more accurate and easier to implement than the EKF. Thus, the UKF has a higher accuracy over the EKF in SOC estimation [19]–[21]. The AUKF, with all the advantages of an UKF, adaptively adjusts process noise covariance and measurement noise covariance in the estimation process. In particular, AUKF, used for SOC estimation in this paper, does not increase much computational burden when updating covariance matrices. Computational burden of the EKF and UKF, however, is still an important consideration in practical applications.

The prerequisite of achieving a highly accurate SOC by the AUKF is the construction of a precise battery model. Hence, a least-square support vector machine (LSSVM) [22] is applied in this research to build the nonlinear battery model with limited initial training samples, which is different from other AUKF-based SOC estimation methods in the literature [19]–[21]. In this paper, a moving window method is proposed for collecting enough training samples. The moving widow can limit the size of dataset to reduce computational burden and select data closely related to the current state to improve estimation accuracy. Since ageing of the battery leads to changes in battery internal characteristics [23], and the parameters of the model vary with SOC level in charging and discharging processes, the battery model should vary with operating time for better accuracy. On the basis of the proposed algorithm, the battery model is not restricted by the structure of equivalent circuit and can be updated during operation. The LSSVM model increases the accuracy of the estimated SOC by acting as the measurement equation in an AUKF. Furthermore, the entire estimation process can be accomplished with a limited number of initial training samples, and desirable results are guaranteed. Simulation and experiment results demonstrate the validity and accuracy of the proposed algorithm in this paper.

This paper is organized as follows. The battery modeling method, which is based on limited training samples by combining the moving window method and LSSVM, is described in Section II; the SOC estimation algorithm based on the AUKF presented in Section III; and the accuracy of the battery modeling method tested in simulation in Section IV; Section V describes the laboratory prototype and presents experimental results using a lithium polymer battery; and the conclusion made in Section VI.

II. Battery Modeling

Battery SOC is the ratio of remaining capacity Q_t to nominal capacity Q_n at the specified discharging rate

$$X_t = \frac{Q_t}{Q_n} \tag{1}$$

Q_t is derived from the integration of current in the discharging process and given by

$$Q_t = Q_0 - \int_0^t \eta \cdot i(\tau) d\tau \tag{2}$$

where Q_0 is the initial capacity, $i(\tau)$ is the instantaneous current at time τ, and η is equal to 1/3600.

Equation (2) is then discretized to be applied to an iterative process as follows:

$$Q_{k+1} = Q_k - \eta \cdot \Delta t \cdot i_k \tag{3}$$

where Q_k and Q_{k+1} represent the remaining battery capacities at time k and $k+1$, respectively, i_k is the battery discharging current, and Δt is the time interval.

As SOC is proportional to Q_t in (1), the state function is shown as follows:

$$X_{k+1} = X_k - \frac{\eta}{Q_n} \cdot \Delta t \cdot i_k \tag{4}$$

where X_k is the battery SOC. Consequently, SOC is derived by integrating the current. However, the Ampere hour counting method has several disadvantages as described in the previous section.

A wide variety of battery models are used in the literature [24]. The models developed by Shepherd, Unnewehr, and Nernst [25] rely on empirical formulas, while equivalent circuit models [26], [27], like the Thevenin battery model, and the electrochemical models are also used for SOC estimation in some literature [28]–[32]. Since the circuit topology and parameters of these models are usually constants, these models only demonstrate their efficiency and accuracy under specified circumstances. However, to achieve a better result in an AUKF, it is necessary to build a precise battery model as measurement equation, which is achieved by the LSSVM [33] in this paper.

In general, the LSSVM algorithm for regression can be formulated as follows [34]:

$$y(x) = \sum_{i=1}^{N} \alpha_i K(x, x_i) + b \tag{5}$$

where α_i is the weight coefficient, b is the bias term, and $K(x, x_i)$ is the kernel function that maps the input data to a higher dimensional space. The radial basis function (RBF) is a popular kernel function in SVM and can accomplish nonlinear mapping [35], [36]. Accordingly, RBF is selected as the kernel function in this paper and expressed as

$$K(x, x_i) = e^{\frac{\|x - x_i\|^2}{2\sigma^2}} \tag{6}$$

where σ is the tuning parameter associated with the RBF kernel function.

Generally, voltage and current are considered as the most influential factors related to SOC in battery charging and discharging processes. Hence, voltage is selected as output variable Z_k and current as input i_k for the measurement equation. The LSSVM model describes the relationship between Z_k and i_k to act as the measurement equation in the AUKF. The two level structure of the LSSVM is illustrated in Fig. 1.

For LSSVM training purpose, a number of samples need to be collected first. Thus, the moving window method is proposed to build the LSSVM model. The moving window method can update the dataset for the training of the LSSVM in the iterative process, expressed as (7) [13], [37], [38]. $w(k)$ is the coefficient multiplied by the training sample. When in the range of the

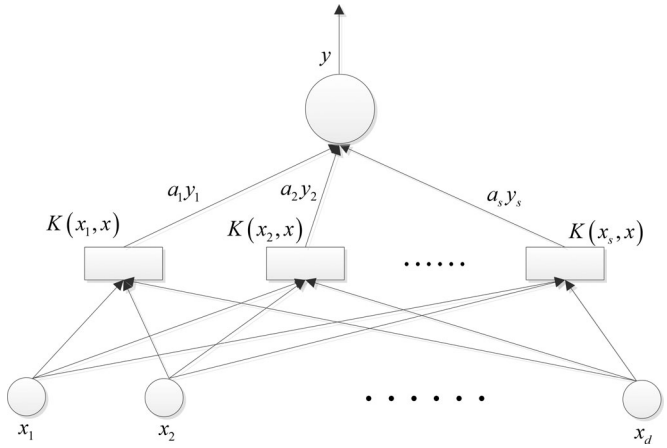

Fig. 1. Structure of LSSVM.

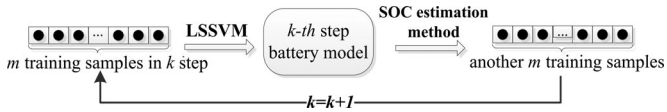

Fig. 2. Flow chart of the moving window method.

moving window, the samples are multiplied by 1. Otherwise, they are multiplied by 0, which means only the samples in the range of the window are selected to train the LSSVM model. Thus, the moving window method is capable of limiting the size of training samples and updates the training samples step by step

$$w(k) = \begin{cases} 1, & 1 < n < M \\ 0, & \text{other.} \end{cases} \tag{7}$$

It is assumed that the number of initial samples is *m*, and the width of the moving window is also defined to *m*. When the moving window method is iterating from *k* to $k+1$ step, the SOC estimation method will yield another *m* samples. The *m* samples in $k+1$ step are applied to train the $(k+1)$th model to reduce computation burden so that the $(k+1)$th model can be used in the next iteration. The iteration procedure of the moving window method is shown in Fig. 2. The method is particularly useful in the case that only a limited number of training samples are obtained at the start of the estimation. Moreover, the battery model can be retrained after sufficient samples are collected in enough iteration steps.

III. Estimation Algorithm Based on AUKF

Using the sampling method to approximate nonlinear distribution makes it possible that UKF could have better estimation results than the EKF. In addition, AUKF does not require computation of the Jacobian matrix and can adaptively adjust process and measurement noise covariances. An accurate SOC by using AUKF has been obtained in conjunction with the measurement equation explained in Section II.

The state-space equation of the battery needs to be established first to start AUKF-based SOC estimation. The measurement equation established by the LSSVM inevitably contains errors due to limited training samples. In addition, errors may also occur in every measurement of the voltage and current. Therefore, system noise q_k and measurement noise r_k are added to state space

$$X_{k+1} = f(X_k, i_k) + q_k = X_k - \frac{\eta}{Q_n} \cdot \Delta t \cdot i_k + q_k \tag{8}$$

$$Z_{k+1} = H(X_k, i_k) + r_k. \tag{9}$$

Equation (8) is directly derived from (4). Equation (9) is the LSSVM model, which acts as the measurement equation in the state-space equation. Equation (8) indicates the relationship between voltage and SOC, with $H(X_k, i_k)$ shown as follows:

$$H(X_k, i_k) = \sum_{i=1}^{l} a_i K(x_i, i_j) + b \tag{10}$$

where $K(x_i, x)$ is the kernel function. a_i and b are the coefficients obtained in the LSSVM training process.

Based on the aforementioned established state-space equation, the AUKF algorithm can be used for SOC estimation.

Step1. *Initialization:* Initial values are calculated by the following equation:

$$\hat{X}_0 = E(X_0) \tag{11}$$

$$P_0 = E\left[\left(X_0 - \hat{X}_0\right) \cdot \left(X_0 - \hat{X}_0\right)^T\right] \tag{12}$$

where X_0 is the initial SOC, and P_0 is the initial posterior error covariance. r_0 and q_0 determine the initial measurement noise covariance and process noise covariance.

Step 2. *Calculation of Sigma Points and Weighting Coefficients:* Sigma points are calculated as follows:

$$\begin{cases} \tilde{X}_0 = \hat{X}_{k-1} \\ \tilde{X}_{k-1}^{(i)} = \hat{X}_{k-1} + \left(\sqrt{(n+\kappa)P_k}\right)_i \\ \tilde{X}_{k-1}^{(j)} = \hat{X}_{k-1} - \left(\sqrt{(n+\kappa)P_k}\right)_{j-n} \end{cases} \tag{13}$$

where *i* is from 1 to *n*, *j* ranges from $n+1$ to 2*n*, and $(\sqrt{(n+\kappa)P_k})_i$ is the *i*th row of the square-rooting matrix.

The calculation of the weighting coefficients in an AUKF is given by

$$\begin{cases} W_m^{(0)} = \kappa/(n+\kappa) \\ W_c^{(0)} = \kappa/(n+\kappa) + \left(1 - \alpha^2 + \beta\right) \\ W_m^{(i)} = W_c^{(i)} = \kappa/[2 \cdot (n+\kappa)] \end{cases} \tag{14}$$

where *n* is the dimension of X_k, and *i* is in the 1–2*n* range. Three additional parameters α, β, and κ are required in (14). α determines the distribution of sigma points, ranging from $1e^{-4}$ to 1 in general. λ is typically selected to be 0 or 3–*n*. β is the state distribution parameter, which is 2 for Gaussian distribution and 0 for single state variable. κ is given by

$$\kappa = a^2(n + \lambda). \tag{15}$$

Step 3. *Prediction and Correction:* Prediction equations are shown as follows:

$$X_{k|k-1}^{(i)} = f\left(\tilde{X}_{k-1}^{(i)}, i_k\right) \tag{16}$$

$$\hat{X}_{k|k-1} = \sum_{i=0}^{2n} W_m^{(i)} \cdot X_{k|k-1}^{(i)} \tag{17}$$

$$P_{x,k|k-1}^{-} = \sum_{i=0}^{2n} W_c^{(i)} \left[X_{k|k-1}^{(i)} - \hat{X}_{k|k-1}\right] \times \left[X_{k|k-1}^{(i)} - \hat{X}_{k|k-1}\right]^T + q_{k-1} \tag{18}$$

$$Z_{k|k-1}^{(i)} = H\left(\hat{X}_{k|k-1}, i_k\right) \tag{19}$$

$$\hat{\mathrm{Z}}_{k|k-1} = \sum_{i=0}^{2n} W_m^{(i)} \cdot Z_{k|k-1}^{(i)}. \tag{20}$$

Correction equations are given by

$$P_{y,k} = \sum_{i=0}^{2n} W_c^{(i)} \left[Z_{k|k-1}^{(i)} - \hat{Z}_{k|k-1}\right] \times \left[Z_{k|k-1}^{(i)} - \hat{Z}_{k|k-1}\right]^T + r_{k-1} \tag{21}$$

$$P_{xy,k} = \sum_{i=0}^{2n} W_c^{(i)} \left[X_{k|k-1}^{(i)} - \hat{X}_{k|k-1}\right] \times \left[Z_{k|k-1}^{(i)} - \hat{Z}_{k|k-1}\right]^T \tag{22}$$

$$K = P_{xy,k} P_{y,k}^{-1} \tag{23}$$

$$\hat{X}_k = \hat{X}_{k|k-1} + K\left(Z_k - \hat{Z}_{k|k-1}\right) \tag{24}$$

$$P_k = P_{x,k|k-1}^{-} - K P_{y,k} K^T. \tag{25}$$

Step4. *Adjustment Process:* The noise covariances q_{k-1} and r_{k-1} are updated by the following equation:

$$\varepsilon_k = Z_k - H(\hat{X}_k, i_k) \tag{26}$$

$$c_k = \frac{\sum_{i=k-L+1}^{k} \varepsilon_i \varepsilon_i^T}{L} \tag{27}$$

$$r_k = c_k + \sum_{i=0}^{2n+1} W_c^{(i)} (Z_{k|k-1}^{(i)} - Z_k + c_k) \times (Z_{k|k-1}^{(i)} - Z_k + c_k)^T \tag{28}$$

$$q_k = K c_k K^T \tag{29}$$

where $\hat{X}_k$ is the estimated SOC by an AUKF in *k*th iteration.

Fig. 3 is the structure of the AUKF algorithm.

The flowchart of the overall algorithm is illustrated in Fig. 4.

In Fig. 4, *m* is the number of the initial training samples, *N* determines whether the number of training samples is enough or not, *t* stands for the operating time of battery, and *T* represents the threshold that determines the updating cycle time of the battery model.

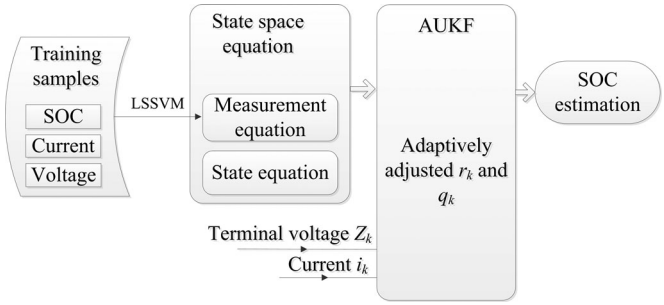

Fig. 3. Schematic diagram of proposed algorithm.

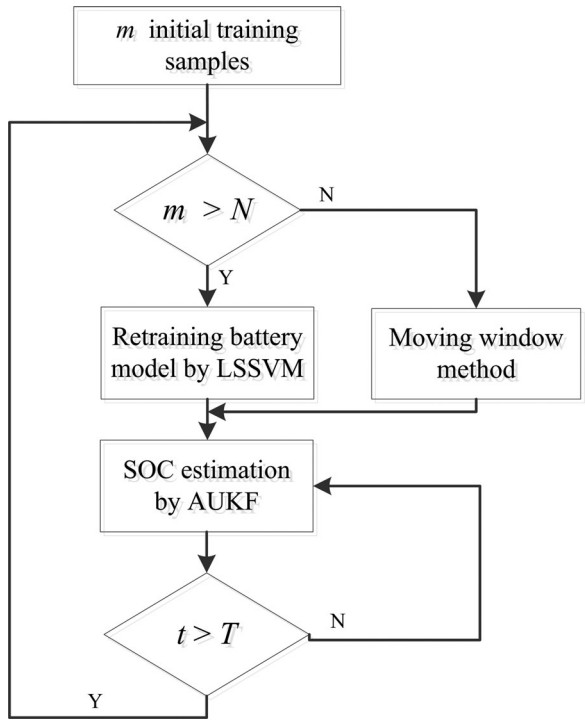

Fig. 4. Flowchart of overall algorithm.

TABLE I
PARAMETERS OF BATTERY MODEL

Nominal Capacity	4.180 Ah
Nominal Voltage	3.338 V

IV. ACCURACY OF LSSVM-BASED MODEL

To verify the accuracy of the LSSVM-based model, simulation tests are designed in this section with the lithium battery model from the research in [39]. Table I shows the battery parameters. Samples are collected for LSSVM training purpose after running the model in Fig. 5.

A specific current profile in Fig. 6(a) is used as discharging current for the battery model in Simulink. The discharging

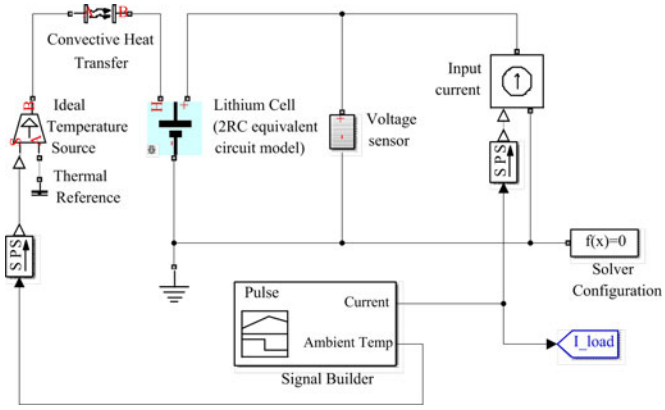

Fig. 5. Lithium battery model in Simulink.

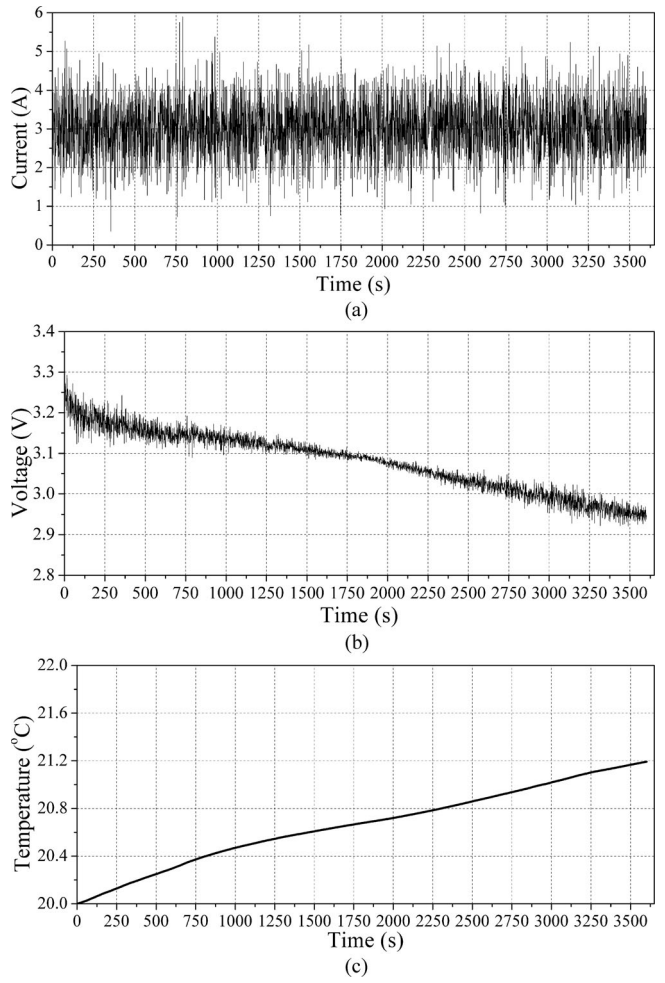

Fig. 6. Physical quantities changes of battery model in Simulation 1, (a) Discharging current, (b) Voltage, (c) Temperature.

current rapidly fluctuates between 0 and 6 A. The voltage, temperature, and SOC are recorded in this test for 3600 s with 1-s sample time. During the discharging process, battery voltage constantly decreases as shown in Fig. 6(b). The cross-validation method is applied for LSSVM parameter optimization.

In order to validate the moving window method in simulation, it is assumed that training samples are not sufficient at the

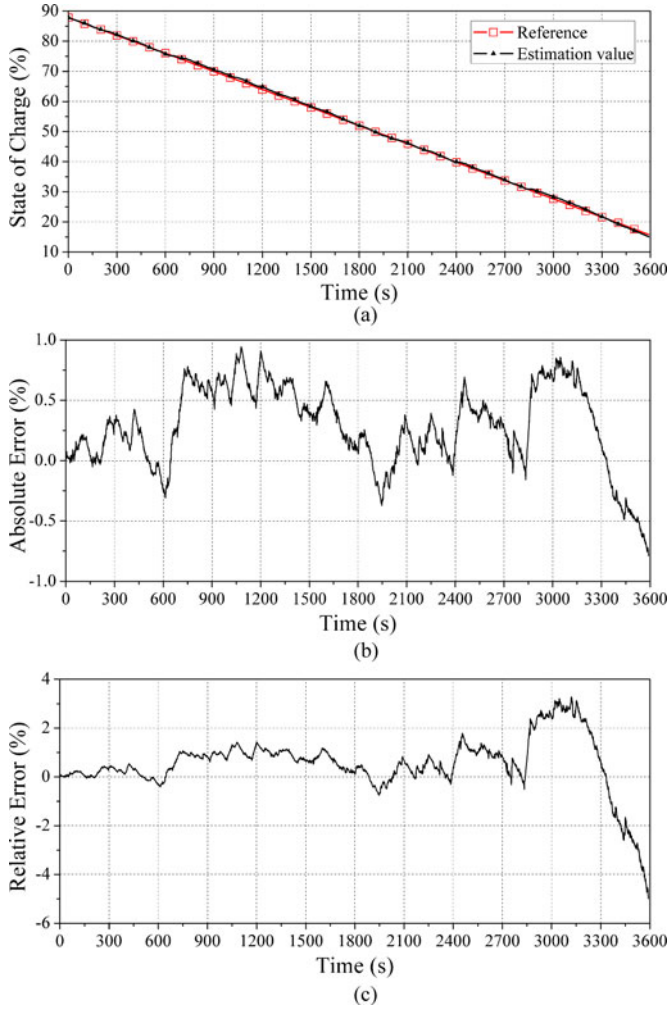

Fig. 7. Test result of moving window method in Simulation 1, (a) State of charge, (b) Absolute errors e_a of SOC, (c) Relative errors e_r of SOC.

beginning of the estimation. The numbers of initial samples m are set to 10, which means only ten SOC values are essential to build the LSSVM model at the start. AUKF is selected as the estimation method so that the required SOC can be obtained in the next iteration. It can be clearly seen from Fig. 7 that the estimated SOC follows its actual values with accuracy.

Two types of errors are used to measure the accuracy of SOC estimation in this paper. Absolute error e_a is defined as

$$e_a = x^* - x \tag{30}$$

where x^* is the approximate value and x is the actual value. In this paper, x^* and x are the estimated SOC and the reference SOC, respectively. As previously described, SOC, as a percentage, represents the ratio of remaining capacity Q_t to nominal capacity Q_n, which means the absolute error e_a is also a percentage.

In this test, the absolute error e_a ranges from -0.79% to $+0.94\%$ as shown in Fig. 7(b). The absolute error e_a in the literature [10], [17] is confined to $\pm 2\%$ error band and $\pm 3\%$ in [11] and [16]. Compared with an average $\pm 15\%$ e_a in the Ampere hour counting method and an average e_a of 5% in the EKF over a wide range of operation [9], the average e_a obtained

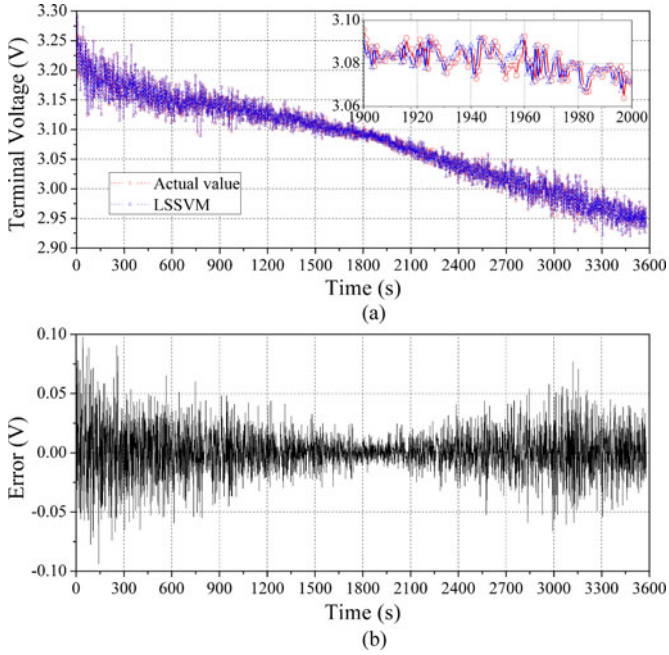

Fig. 8. Test result of retrained measurement equation in Simulation 1, (a) The output of the measurement equation, (b) Errors of measurement equation.

in this test is less than 0.5%, which proves the validity of the moving window method. It can be also seen that the average $|e_a|$ is 0.47% when SOC is below 20% and that the average $|e_a|$ is 0.37% in other SOC ranges. One reason for the increase in e_a is the high nonlinearity of the dependence of model parameters on SOC in lower SOC ranges [5], [12]. Another reason is that the estimated SOC in the current step adopts the model established by the training data in the previous step. The variation of voltage curve [see Fig. 14(b)] is steeper in the lower range of SOC, which inevitably increases the difference between established models in the two steps. Thus, the increase in e_a and e_r is mainly due to the nonlinear changes in battery internal characteristics and the updated mode of the moving window method. However, compared with the results in the literature [10], [11], [16], [17], the variation curve of e_a in this paper does not increase significantly at lower SOC level and e_a is always less than $\pm 2\%$ in overall SOC ranges.

In addition to the absolute error, the relative error e_r can be defined as

$$e_r = \frac{x^* - x}{x} \tag{31}$$

where x^* is the approximate value and x is the actual value.

When SOC is below 20% at 3370 s, the relative error e_r increases faster than SOC level in the range of 100%–20%. The relative error e_r is between -3.3% and $+4.99\%$, as shown in Fig. 7(c). Despite the reasons explained earlier, the increase in e_r mainly results from the decrease in denominator (low SOC value) in (31). Thus, the resulting e_r is higher in lower SOC ranges, the average $|e_r|$ for SOC below 20% can reach nearly 3% and the maximum $|e_r|$ is around 5%. Although e_a and e_r increase when SOC is below 20%, the proposed method can still

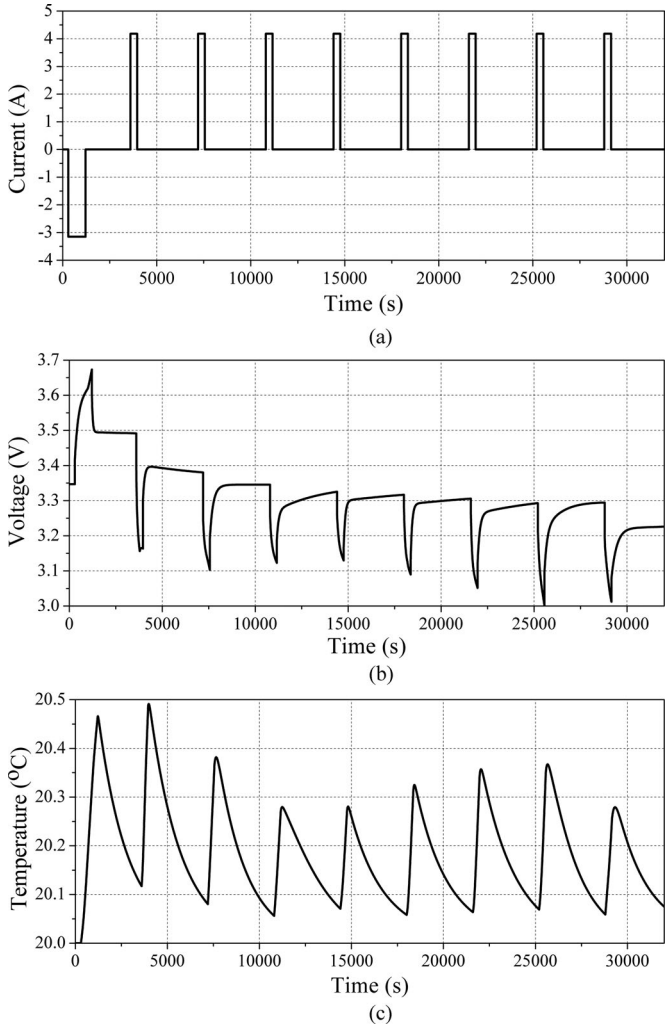

Fig. 9. Physical quantity changes of battery model in Simulation 2, (a) Discharging current, (b) Voltage, (c) Temperature.

be used to obtain acceptable results compared with the literature [10], [11], [16], [17].

Since battery parameters vary with time and modeling precision depends on the number of training samples, the established measurement equation needs to be updated after a period of operating. The LSSVM model is retrained after 3600 training samples are collected in this test. The LSSVM model output is compared with the measured voltage to examine the accuracy of the proposed modeling method. It can be seen that the voltages calculated by the retrained LSSVM model are close to the actual values in Fig. 8(a). Most errors are less than 0.1 V in Fig. 8(b), which indicates the high accuracy of the developed model.

It is also necessary to investigate the moving window method in slower current profiles due to the importance of the internal dynamic phenomena of batteries. Another test is designed in simulation to validate the performance of the modeling method in slower current profiles, with sampling time also set to 1 s. As shown in Fig. 9(a), the discharging current profile is slower than it is in the previous test, and the negative current represents the charging current as well. The estimated SOC closely follows their reference values in the whole process, as shown in

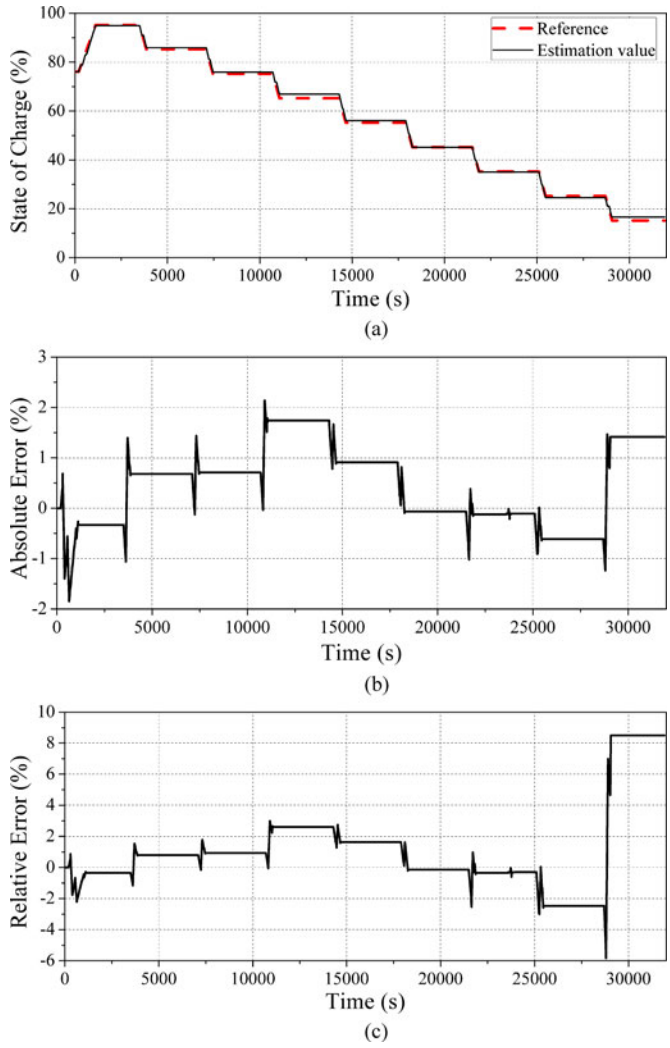

Fig. 10. Test result of moving window method in Simulation 2, (a) State of charge, (b) Absolute errors e_a of SOC, (c) Relative errors e_r of SOC.

Fig. 10(a). It can be seen from Fig. 10(b) that the absolute error $|e_a|$ of the estimated SOC value is less than 1%. The proposed moving window method in slower current profiles achieves expected performance in estimation accuracy. However, the average $|e_r|$ in Fig. 10(c) still increases to more than 9% for SOC below 20%, due to the smaller value of denominator reference (low SOC value).

As mentioned previously, in order to achieve better accuracy, the LSSVM model is retrained with enough samples collected in this test. The LSSVM model output is then compared with the actual voltages in Fig. 11. The errors are less than 0.1 V in most cases, which indicates the accuracy of the LSSVM model in slower current profiles.

V. Experimental Results

The moving window modeling technique and the AUKF-based estimation method are applied to real applications, and the experimental results are shown in this section. A lithium polymer battery manufactured by KOKAM Company is used to

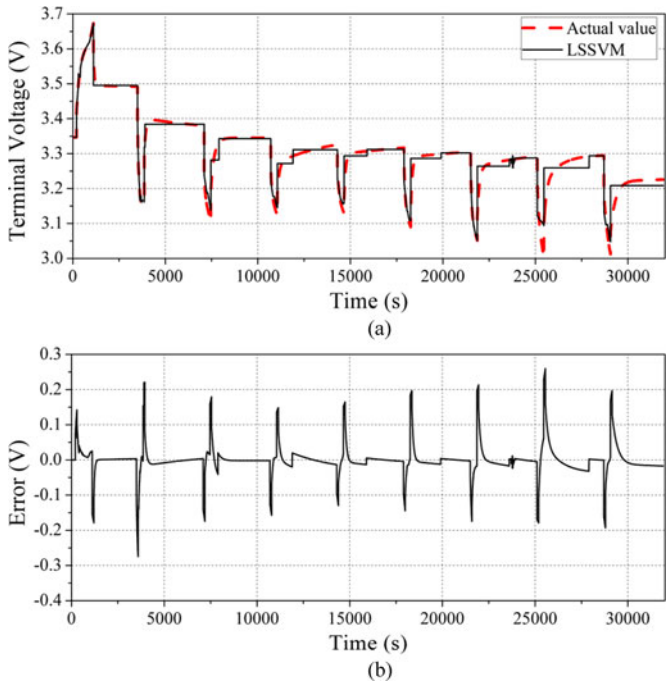

Fig. 11. Test result of retrained measurement equation in Simulation 2, (a) Output of measurement equation, (b) Errors of measurement equation.

TABLE II
Parameters of the Lithium Polymer Battery

Nominal Capacity	70.0 Ah
Nominal Voltage	3.7 V

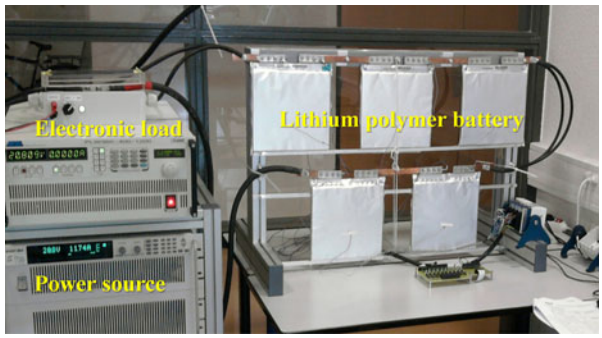

Fig. 12. Test bench.

acquire the dataset. The parameters corresponding to the battery are listed in Table II with the test bench shown in Fig. 12.

The structure of the experimental test bench is shown in Fig. 13. The battery pack to be tested is electrically connected to a programmable power supply and an electronic load. The electronic load can impose a battery discharging cycle, and the programmable power supply can impose a charging cycle (for example, to simulate the regenerative braking of an electric vehicle). Both charging and discharging cycles are generated by a supervision PC and sent to the electronic load and the power supply via digital interfaces (GPIB and RS232). During the test, the individual battery cell current, voltage and temperature are

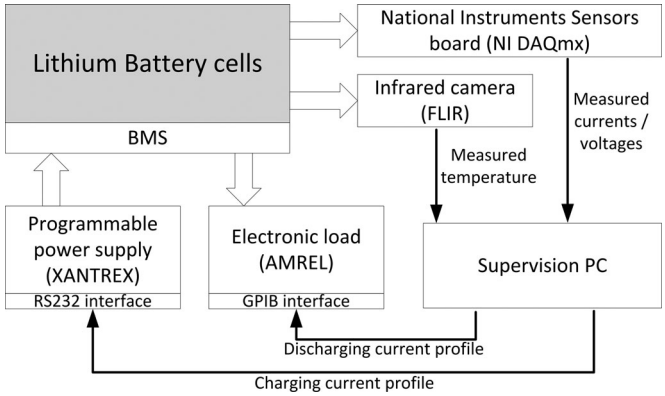

Fig. 13. Test bench system diagram.

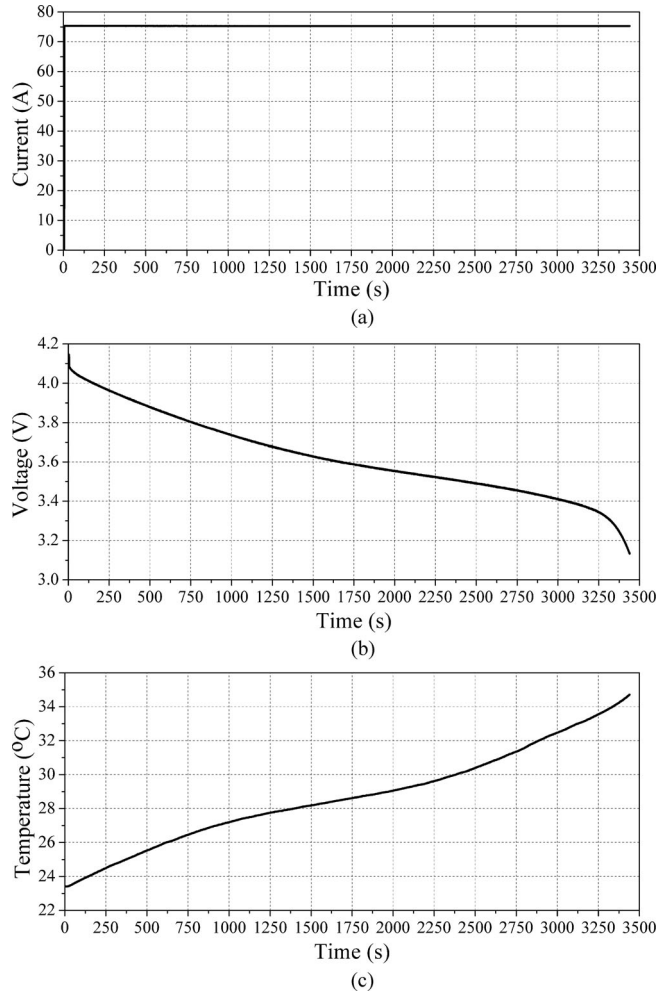

Fig. 14. Physical quantities changes of battery in Experiment 1, (a) Discharging current, (b) Voltage, (c) Temperature

measured by voltage/current sensors and an infrared camera placed in front of the battery cells. The measured data are sent and stored in the supervision PC for subsequent analysis.

To validate the battery in a slower current profile, the lithium polymer battery is discharged with the current shown in Fig. 14(a). The current is 75 A, which is almost a constant value

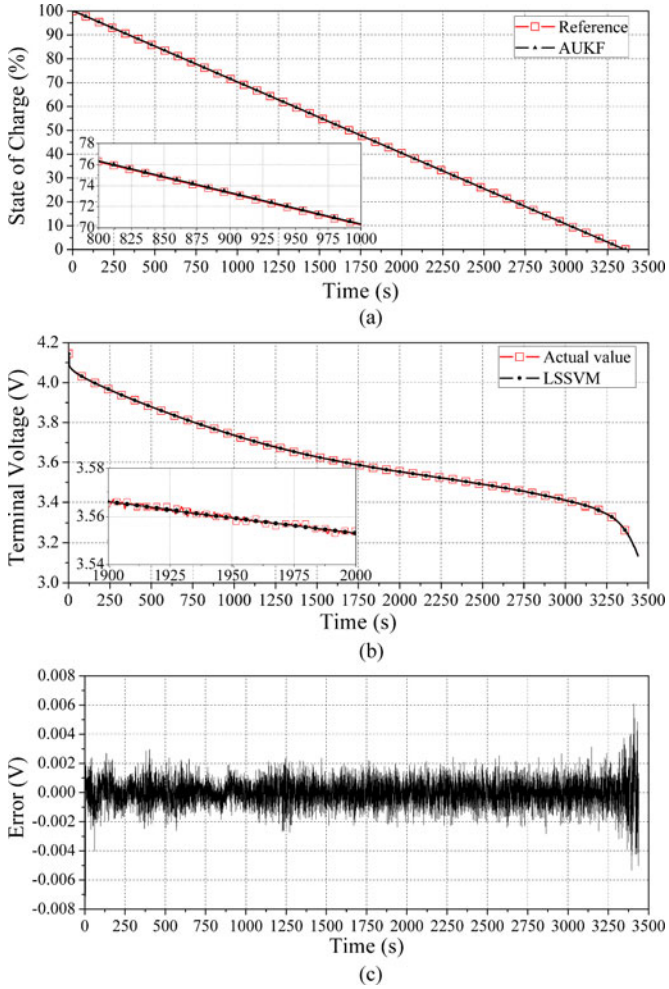

Fig. 15. Test result of measurement function in Experiment 1, (a) State of charge, (b) Voltage, (c) Errors.

in the entire discharging process. The voltage and temperature of the battery slowly change as shown in Fig. 14(b) and (c). The discharging process lasts for 3440 s with sampling time 0.4 s.

The accuracy of the modeling method has been proved in simulation environment. In this section, the method is applied to experimental test. The window width m is set to 10, the same as in Simulation 1. The results in Fig. 15(a) show the SOC estimated by the AUKF and the moving window method is also applied in the discharging process. The estimated SOC is very close to the reference values, which indicates the accuracy of the method in slower current profiles. Afterward, the estimated SOC and the measured quantities are used to train a new battery model. The voltage calculated by the LSSVM model is compared with the measured voltage to validate the new measurement equation. The calculated values are almost in agreement with the measured values in Fig. 15(b). The errors of the method are negligible in Fig. 15(c), which further confirms the validity of the moving window method.

Subsequently, experiments are also conducted to validate the moving window method in fast dynamic current profiles. The range of the discharging current is from -224 to 396 A in

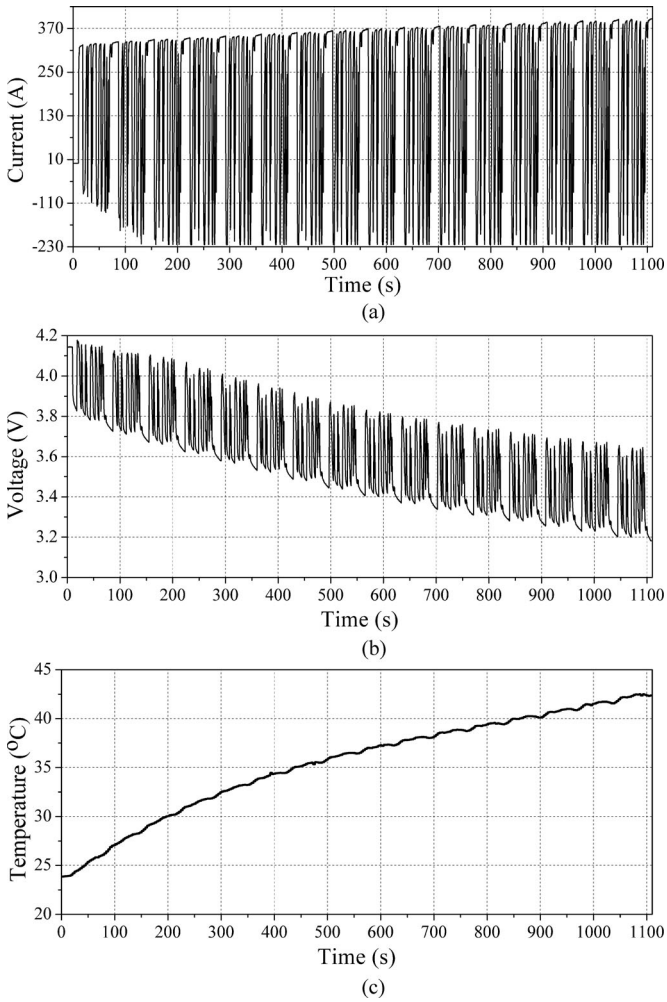

Fig. 16. Physical quantities changes of battery in Experiment 2, (a) Discharging current, (b) Voltage, (c) Temperature.

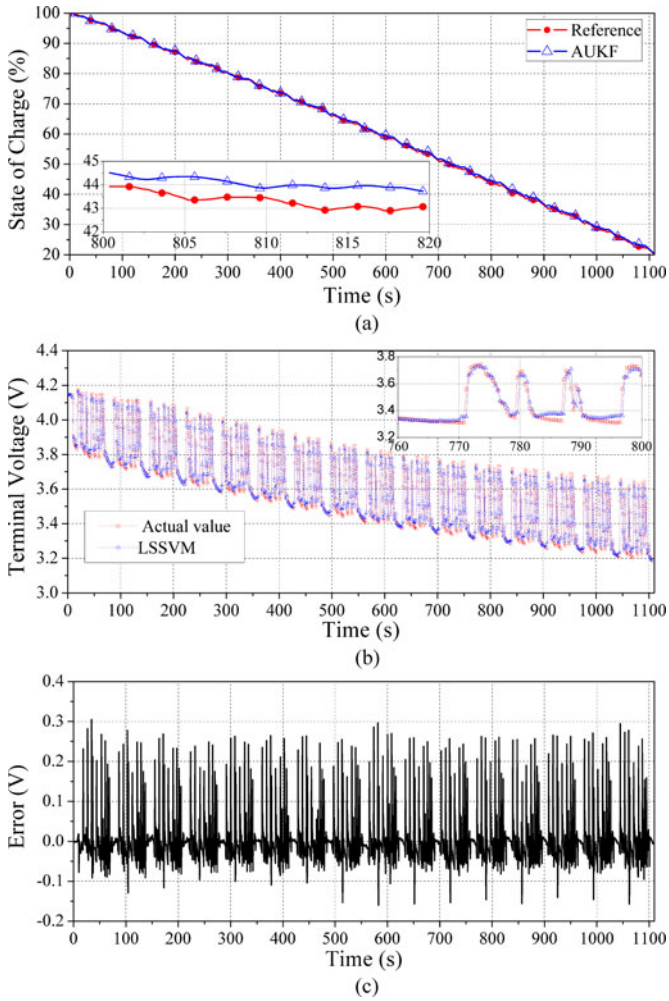

Fig. 17. Test result of measurement function in Experiment 2, (a) State of charge, (b) Voltage, (c) Errors.

Fig. 16(a), while the negative discharging current actually represents the battery charging current. The variations of voltage and temperature are shown in Fig. 16(b) and (c). The battery is continuously discharging for 1108 s. Moreover, the sampling interval of current and voltage is 0.4 s.

The moving window width $m = 10$ is also chosen. Fig. 17(a) shows the estimated SOC by the moving window method. And the model can be retrained after enough training samples have been collected. The calculated voltages of the measurement equation are compared with the measured voltages in Fig. 17(b). Most errors in Fig. 17(c) are less than 0.2 V, which indicates a high accuracy of the modeling method.

The accuracy of the moving window modeling method has been validated by both simulation and experiment. Afterwards, the retrained model is used as the measurement equation in the AUKF to estimate the battery SOC. The AUKF-based method is compared with an UKF to validate its performance in experiment. In addition to using the LSSVM model trained by SOC reference values, the model based on SOC estimation values is also applied to an AUKF. Essentially, the two models are trained by different sources of SOC. The reference value of SOC is obtained from the experimental test bench (AUKF based on actual value in Fig. 18), while SOC estimation value is collected by the moving window modeling method (AUKF based on estimation value in Fig. 18). Considering the difficulty to get initial SOC in real conditions, the initial SOC could be set to a reasonable value arbitrarily. Thus, the value of initial SOC is set to 50% for both estimation methods in this experiment. The mean absolute error (MAE) of the results is calculated by

$$e_{\mathrm{mae},k} = \frac{\sum_{i=0}^{k} \left| X_i - \hat{X}_i \right|}{k+1}. \tag{32}$$

The comparative results of different methods are shown in Fig. 18, and the estimation results of both methods follow the trend of reference values, though errors can always be observed in Fig. 18(a). The MAE of the estimated SOC is reduced to less than 5% at the end of the curves in Fig. 18(b), which proves the effectiveness of the UKF and AUKF. However, the convergence speed of the AUKF is still higher than that of the UKF and AUKF errors are clearly less than those of the UKF as shown in Fig. 18(b), which indicate the superiority of the AUKF to UKF.

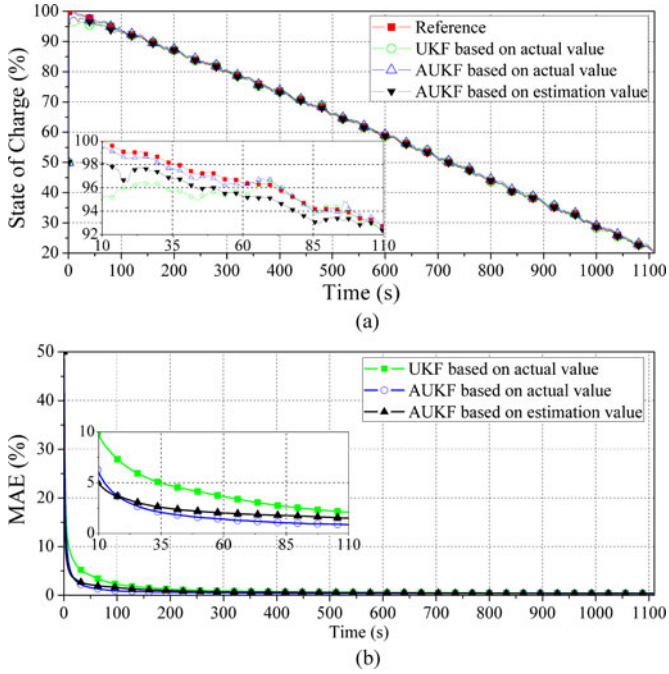

Fig. 18. Experimental results and MAE of methods in Experiment 2, (a) State of charge, (b) MAE.

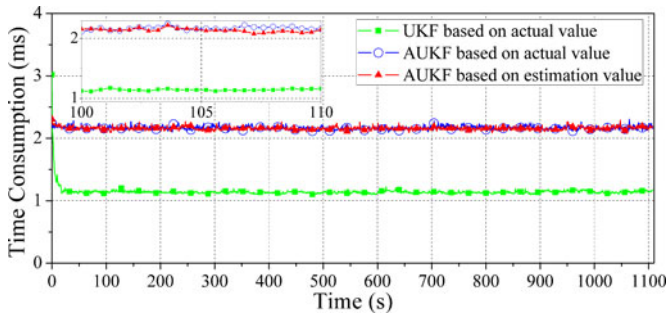

Fig. 19. Time consumption of different methods in Experiment 2.

The AUKF based on estimation value of SOC also obtains good results in Fig. 18. The MAE is almost the same for the two AUKF-based methods, which indicates the effectiveness of the proposed method.

Since computational burden plays an important role in real applications, it is also quite necessary to pay attention to the time consumption of the Kalman filter-based methods. In order to quantify the computational cost, the experiment is repeated for ten times to calculate the average time consumption. The results in Fig. 19 show the average values for each iteration, which indicates that an AUKF consumes more time than an UKF. The calculated average values and maximum value of time consumption for different methods are shown in Table III, which explicitly indicates that an UKF is almost twice as fast as an AUKF in the experiment.

The proposed method needs to be applied to another experiment to further test its performance on accuracy for SOC below 20%. In Experiment 3, the battery is discharged until its SOC is 10%. The variations of voltage, current, and temperature in the process are shown in Fig. 20. The current changes rapidly from –110 to 430 A, while the lasting time of experiment is still 1108 s. The negative discharging current in the figure represents the charging current of the battery.

TABLE III
TIME CONSUMPTION OF DIFFERENT METHODS

Method	Mean of time consumption (ms)	Maximum value of time consumption (ms)
UKF	1.1424	3.0201
AUKF based on actual value	2.1665	2.3467
AUKF based on estimation value	2.1605	2.3317

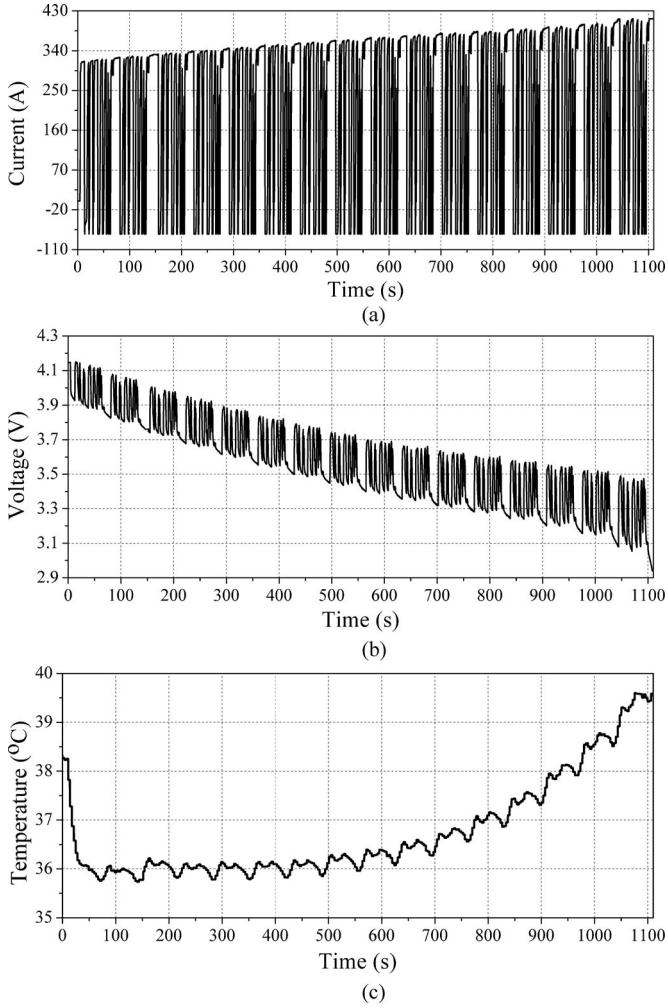

Fig. 20. Physical quantities changes of battery in Experiment 3, (a) Discharging current, (b) Voltage, (c) Temperature.

The initial SOC is set to 20% for all methods in the experiment. When the same battery model is used as the measurement equation, the AUKF-based method approaches the reference values faster than an UKF, as illustrated in Fig. 21(a). The AUKF based on estimation value of SOC also follows the references, which can be seen in Fig. 21(a). The MAE is less than 5% after

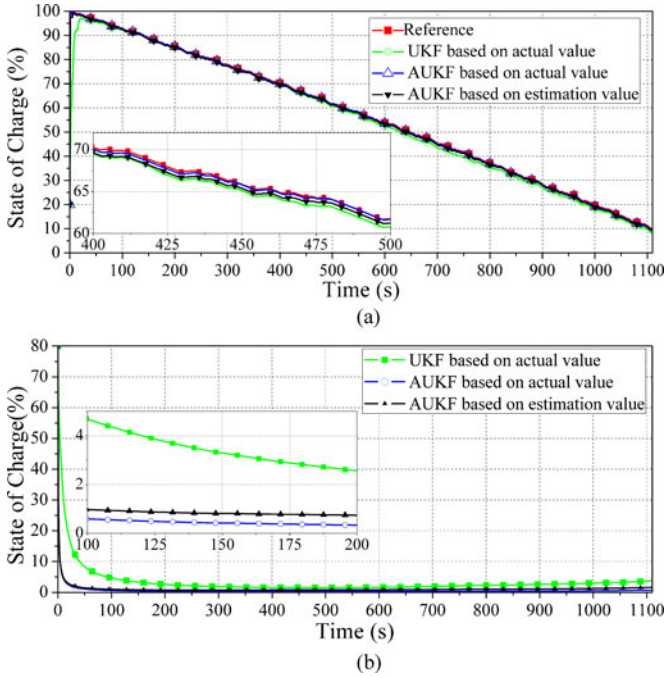

Fig. 21. Experimental results and MAE of methods in Experiment 3, (a) State of charge, (b) MAE.

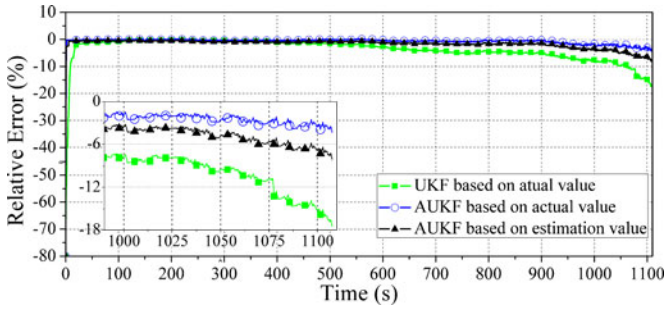

Fig. 22. Relative errors in estimation process.

TABLE IV
AVERAGE ERRORS OF ALGORITHMS IN DIFFERENT SOC LEVEL

Method	$\lvert e_r \rvert$ (SOC $<$ 20%)	$\lvert e_a \rvert$ (SOC $<$ 20%)	$\lvert e_r \rvert$ (SOC $\geq$ 20%)	$\lvert e_a \rvert$ (SOC $\geq$ 20%)
UKF	10.5%	1.54%	3.0%	1.5%
AUKF based on actual value	2.5%	0.38%	0.5%	0.24%
AUKF based on estimation value	5.0%	0.73%	1.2%	0.63%

a certain number of iterations in Fig. 21(b), which indicates the effectiveness of the proposed method.

Fig. 22 shows the relative error e_r for each step in Experiment 3. It can be confirmed that SOC estimation relative errors e_r increase for SOC below 20% in the subgraph of Fig. 22. In Table IV, the average $|e_r|$ and $|e_a|$ also increase in the same condition. However, the AUKF-based method still obtains better accuracy than an UKF. The results indicate that an AUKF

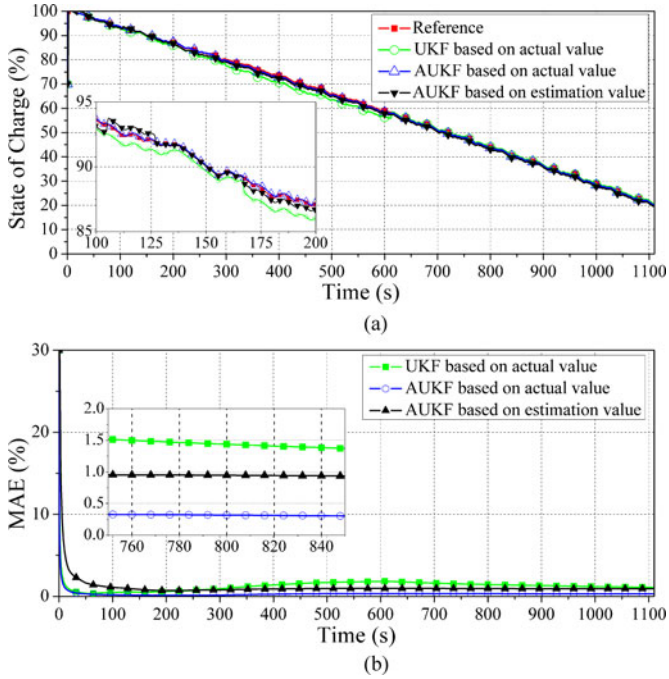

Fig. 23. Experimental results and MAE with separate datasets for model identification and validation, (a) State of charge, (b) MAE.

using estimation values of SOC is not as good as the results from an AUKF using actual values, but the result is reasonable and acceptable. As described previously, the two AUKF-based methods use different sources of SOC, resulting in the difference in accuracy.

Then, separate datasets are used for model identification and validation. The model is established by samples in Experiment 2 and validated by dataset in Experiment 3. The initial SOC is set to 70% in the experiment.

The estimated SOC follows their reference in Fig. 23(a) and the MAE is less than 5% in Fig. 23(b), which indicate the validity of the proposed method in separate datasets for model identification and validation.

VI. CONCLUSION

A highly accurate algorithm for lithium polymer battery SOC estimation is presented with a limited number of initial training samples. In order to solve the problem of lacking training data, moving window modeling method is proposed to build the LSSVM model. The width of the moving window is set to 10 in Section V, i.e., only 10 initial values are needed to start the estimation. The simulation and experiment results of the estimated SOC closely follow their reference values. As internal dynamic phenomena of the batteries are very important, the modeling method is also tested in both slow and fast dynamic current profiles, with results showing high accuracy of the moving window modeling method in different variations of current profile.

With enough data collected using the moving window method, the LSSVM-based model is cyclically updated to improve its accuracy. Accordingly, an accurately retrained battery

model is obtained, which is validated by comparing the output of the model with measured voltages in the simulation and experiment.

The LSSVM-based measurement equation is used in an AUKF. Experimental results validate the proposed AUKF algorithm in different initial SOCs. Additionally, separate datasets are adopted for model identification and validation. The average absolute error is less than 2%, which proves the feasibility and accuracy of the algorithm. Furthermore, as an LSSVM is a universal method, the proposed method is able to be applied to other battery types as well.

With computational burden being crucial to Kalman-filter-based methods, the experiment section lists the time consumption of the proposed method. Future work is expected to aim at reducing its computational burden.

REFERENCES

[1] K. Rajashekara, "Present status and future trends in electric vehicle propulsion technologies," *IEEE J. Emerg. Sel. Topics Power Electron.*, vol. 1, no. 1, pp. 3–10, Mar. 2013.

[2] T. Kim, W. Qiao, and L. Qu, "Power electronics-enabled self-X multicell batteries: A design toward smart batteries," *IEEE Trans. Power Electron.*, vol. 27, no. 11, pp. 4723–4733, Nov. 2012.

[3] L. Lu, X. Han, J. Li, J. Hua, and M. Ouyang, "A review on the key issues for lithium-ion battery management in electric vehicles," *J. Power Sources*, vol. 226, pp. 272–288, 2013.

[4] W. C. Lee and D. Drury, "Development of a hardware-in-the-loop simulation system for testing cell balancing circuits," *IEEE Trans. Power Electron.*, vol. 28, no. 12, pp. 5949–5959, Dec. 2013.

[5] N. Lotfi, P. Fajri, S. Novosad, J. Savage, R. G. Landers, and M. Ferdowsi, "Development of an experimental testbed for research in lithium-ion battery management systems," *Energies*, vol. 6, pp. 5231–5258, 2013.

[6] Y. M. Jeong, Y. K. Cho, J. H. Ahn, S. H. Ryu, and B. K. Lee, "Enhanced Coulomb counting method with adaptive SOC reset time for estimating OCV," in *Proc. IEEE Energy Convers. Congr. Expo.*, Pittsburgh, PA, USA, Sep. 14–18, 2014, pp. 1313–1318.

[7] M. Petzl and M. A. Danzer, "Advancements in OCV measurement and analysis for lithium-Ion batteries," *IEEE Trans. Energy Convers.*, vol. 28, no. 3, pp. 675–681, Sep. 2013.

[8] Y. S. Lee, W. Y. Yang, and T. Y. Kuo, "Soft computing for battery state-of-charge estimation in battery string systems," *IEEE Trans. Ind. Electron.*, vol. 55, no. 1, pp. 229–239, Jan. 2008.

[9] J. C. Alvarez Anton, P. J. Garcia Nieto, F. J. de Cos Juez, F. Sanchez Lasheras, C. Blanco Viehjo, and N. Roqueni Gutierrez, "Battery state-of-charge estimator using the MARS technique," *IEEE Trans. Power Electron.*, vol. 28, no. 8, pp. 3798–3805, Aug. 2013.

[10] J. Xu, C. C. Mi, B. G. Cao, and J. J. Deng, "The state of charge estimation of lithium-ion batteries based on a proportional-integral observer," *IEEE Trans. Veh. Technol.*, vol. 63, no. 4, pp. 1614–1621, May 2014.

[11] I. S. Kim, "Nonlinear state of charge estimator for hybrid electric battery," *IEEE Trans. Power Electron.*, vol. 23, no. 4, pp. 2027–2034, Jul. 2008.

[12] N. Lotfi and R. G. Landers, "Robust nonlinear observer for state of charge estimation of Li-ion batteries," in *Proc. ASME Dyn. Syst. Control Conf.*, Ft. Lauderdale, FL, USA, Oct. 17–19, 2012, pp. 641–648.

[13] H. Rahimi-Eichi, F. Baronti, and M. Y. Chow, "Online adaptive parameter identification and state-of-charge coestimation for lithium-polymer battery cells," *IEEE Trans. Ind. Electron.*, vol. 61, no. 4, pp. 2053–2061, Apr. 2014.

[14] J. Kim, J. Shin, C. Chun, and B. H. Cho, "Stable configuration of a Li-ion series battery pack based on a screening process for improved voltage/SOC balancing," *IEEE Trans. Power Electron.*, vol. 27, no. 1, pp. 411–424, Jan. 2012.

[15] J. Kim, S. Lee, and B. H. Cho, "Complementary cooperation algorithm based on DEKF combined with pattern recognition for SOC/capacity estimation and SOH prediction," *IEEE Trans. Power Electron.*, vol. 27, no. 1, pp. 436–451, Jan. 2012.

[16] Z. Chen, Y. H. Fu, and C. C. Mi, "State of charge estimation of Lithium-Ion batteries in electric drive vehicles using extended Kalman filtering," *IEEE Trans. Veh. Technol.*, vol. 62, no. 3, pp. 1020–1030, Mar. 2013.

[17] R. Xiong, H. W. He, F. C. Sun, and K. Zhao, "Evaluation on state of charge estimation of batteries with adaptive extended Kalman filter by experiment approach," *IEEE Trans. Veh. Technol.*, vol. 62, no. 1, pp. 108–117, Jan. 2013.

[18] S. J. Julier, J. K. Uhlmann, and H. F. Durrant-Whyte, "A new approach for filtering nonlinear systems," in *Proc. Amer. Control Conf.*, Seattle, WA, USA, Jun. 21–23, 1995, pp. 1628–1632.

[19] F. C. Sun, X. S. Hu, Y. Zou, and S. G. Li, "Adaptive unscented Kalman filtering for state of charge estimation of a lithium-ion battery for electric vehicles," *Energy*, vol. 36, no. 5, pp. 3531–3540, May 2011.

[20] H. Aung, K. S. Low, and S. T. Goh, "State-of-charge estimation of lithium-ion battery using square root spherical unscented Kalman filter (Sqrt-UKFST) in Nanosatellite," *IEEE Trans. Power Electron.*, vol. 30, no. 9, pp. 4774–4783, Sep. 2015.

[21] H. Gholizade-Narm and M. Charkhgard, "Lithium-ion battery state of charge estimation based on square-root unscented Kalman filter," *IET Power Electron.*, vol. 6, pp. 1833–1841, Nov. 2013.

[22] J. A. K. Suykens and J. Vandewalle, "Least squares support vector machine classifiers," *Neural Process. Lett.*, vol. 9, no. 3, pp. 293–200, 1999.

[23] L. Long and P. Bauer, "Practical capacity fading model for Li-ion battery cells in electric vehicles," *IEEE Trans. Power Electron.*, vol. 28, no. 12, pp. 5910–5918, Dec. 2013.

[24] M. Einhorn, F. V. Conte, C. Kral, and J. Fleig, "Comparison, selection, and parameterization of electrical battery models for automotive applications," *IEEE Trans. Power Electron.*, vol. 28, no. 3, pp. 1429–1437, Mar. 2013.

[25] H. A.-H. Hussein and I. Batarseh, "An overview of generic battery models," in *Proc. IEEE Power Energy Soc. Gen. Meeting*, San Diego, CA, USA, Jul. 24–29, 2011, pp. 1–6.

[26] W. G. Wang, H. S.-H. CHUNG, and J. Zhang, "Near-real-time parameter estimation of an electrical battery model with mulitple time consonants and SOC-dependent capacitance," *IEEE Trans. Power Electron.*, vol. 29, no. 11, pp. 5905–5920, Nov. 2014.

[27] N. Kularatna, "Dynamics and modeling of rechargeable batteries: What electrochemists? Work tells the electronic enginners," *IEEE Power Electron. Mag.*, vol. 1, no. 4, pp. 23–33, Dec. 2014.

[28] H. Fang, Y. Wang, Z. Sahinoglu, T. Wada, and S. Hara, "Adaptive estimation of state of charge for lithium-ion batteries," in *Proc. Amer. Control Conf.*, Washington, DC, USA, Jun. 17–19, 2013, pp. 3485–3491.

[29] Y. Wang, H. Fang, Z. Sahinoglu, T. Wada, and S. Hara, "Adaptive estimation of the state of charge for lithium-ion batteries: Nonlinear geometric observer approach," *IEEE Trans. Control Syst. Technol.*, vol. 23, no. 3, pp. 948–962, May 2015.

[30] S. Dey, B. Ayalew, and P. Pisu, "Adaptive observer design for a Li-ion cell based on coupled electrochemical-thermal model," presented at the ASME Dynamic System Control Conf., San Antonio, TX, USA, Oct. 22–24, 2014.

[31] S. Dey, B. Ayalew, and P. Pisu, "Nonlinear robust observers for state-of-charge estimation of lithium-ion cells based on a reduced electrochemical model," *IEEE Trans. Control Syst. Technol.*, to be published.

[32] R. Ahmed, M. EI Sayed, I. Arasaratnam, J. Tjong, and S. Habibi, "Reduced-order electrochemical model parameters identification and SOC estimation for healthy and aged Li-ion batteries Part I: parameterization model development for healthy batteries," *IEEE J. Emerg. Sel. Topics Power Electron.*, vol. 2, no. 3, pp. 659–677, Sep. 2014.

[33] K. D. Brabanter, J. D. Brabanter, J. A. K. Suykens, and B. D. Moor, "Approximate confidence and prediction intervals for least squares support vector regression," *IEEE Trans. Neural. Netw.*, vol. 22, no. 1, pp. 110–120, Jan. 2011.

[34] Q. Xu, "Identification and compensation of piezoelectric hysteresis without modeling hysteresis inverse," *IEEE Trans. Ind. Electron.*, vol. 60, no. 9, pp. 3927–3937, Sep. 2013.

[35] J. C. Alvarez Anton, P. J. Garcia Nieto, F. J. de Cos Juez, F. Sanchez Lasheras, C. Blanco Viehjo, and N. Roqueni Gutierrez, "Support vector machines used to estimate the battery state of charge," *IEEE Trans. Power Electron.*, vol. 28, no. 12, pp. 5919–5926, Dec. 2013.

[36] T. Hacib, Y. Le Bihan, M. K. Smail, M. R. Mekideche, O. Meyer, and L. Pichon, "Microwave characterization using ridge polynomial neural networks and least square support vector machines," *IEEE Trans. Magn.*, vol. 47, no. 5, pp. 990–993, May 2011.

[37] C. Lokan and E. Mendes, "Applying moving windows to software effort estimation," in *Proc. Int. Symp. Empirical Softw. Eng. Meas.*, Lake Buena Vista, FL, USA, Oct. 15–16, 2009, pp. 111–122.

[38] J. Heidrich, M. Oivo, A. Jedlitschka, and M. T. Baldassarre, "The evaluation of weighted moving windows for software effort estimation," in *Product-Focused Software Process Improvement*. Berlin, Germany: Springer, 2013, pp. 214–228.

[39] T. Huria, M. Ceraolo, J. Gazzarri, and R. Jackey, "High fidelity electrical model with Thermal dependence for characterization and simulation of high power lithium battery cells," in *Proc. Electr. Veh. Conf.*, Mar. 4–8, 2012, pp.1–8.

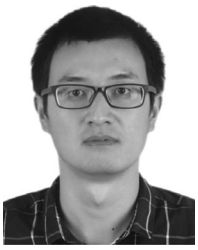

Jinhao Meng (S'14) received the B.S. degree in automation from the Xi'an University of Science and Technology, Xi'an, China, in 2010, and the M.S. degree in control theory and control engineering from Northwestern Polytechnical University, Xi'an, in 2013, where he is currently working toward the Ph.D. degree in electrical engineering.

His research interests include battery modeling, battery status estimation, and energy management of hybrid electric vehicles.

Guangzhao Luo (M'08) received the M.S. and Ph.D. degrees in electrical engineering from Northwestern Polytechnical University (NPU), Xi'an, China, in 1998 and 2003, respectively.

From 2003 to 2004, he was a Postdoctoral in the University of Federal Defense, Munich, Germany. He is currently a Professor with NPU. In addition, he is the Vice Director of the Rare Earth Permanent Magnet Electric Machine and Control Engineering Center of Shaanxi Province. His research interests include advance control theory of permanent magnet electrical machine, high performance control technology of PMSM for electric traction and EV, real-time simulation technology for electrical drive system, and intelligence control of new energy conversion.

Dr. Luo received the second prize of the China National Defense Science and Technology Progress Award in 1995 and 2011, respectively.

Fei Gao (S'09–M'11–SM'15) received the master's degree in electrical and control system engineering, in 2007, and the Ph.D. degree in renewable energy with distinguished youth doctor reward in 2010, both from the University of Technology of Belfort-Montbéliard (UTBM), Belfort, France.

He is currently an Associate Professor at the Energy Department, UTBM, France. He is the Head of the Energy Production Division, Department of Energy, UTBM.

Dr. Gao is the holder of the French research expertise bonus (PEDR) by the French Ministry of Higher Education and Research with A rank. He is also an Associate Editor of the IEEE TRANSACTIONS ON INDUSTRY APPLICATIONS and the IEEE TRANSACTIONS ON TRANSPORTATION ELECTRIFICATION, and the Chair of fuel cell modeling axis of the Fuel Cell Research Federation in France. He is elected in 2013 as Secretary of the Technical Committee on Transportation Electrification of the IEEE Industry Electronic Society.